JBC RESEARCH ARTICLE

# *In vitro* reconstitution reveals substrate selectivity of protein S-acyltransferases

Received for publication, October 14, 2024, and in revised form, February 19, 2025 Published, Papers in Press, March 14, 2025,
https://doi.org/10.1016/j.jbc.2025.108406

**Tanmay Mondal, James Song, and Anirban Banerjee***

*From the Section on Structural and Chemical Biology, Neurosciences and Cellular and Structural Biology Division, Eunice Kennedy Shriver National Institute of Child Health and Human Development, National Institutes of Health, Bethesda, Maryland, USA*

Reviewed by members of the JBC Editorial Board. Edited by Mike Shipston

**Protein S-acylation, commonly known as protein palmitoylation, is the most prevalent form of protein lipidation with ~6000 target proteins and in humans, is catalyzed by 23 integral membrane enzymes of the zDHHC family. Recognition of its importance in cellular physiology as well as human diseases has undergone an explosive growth in recent years. Yet, the nature of zDHHC–substrate interactions has remained poorly understood for most zDHHC enzymes. Cell-based experiments indicate a promiscuous and complex zDHHC-substrate network, whereas lack of *in vitro* reconstitution experiments has impeded insights into the nature of discrete zDHHC–substrate interactions. Here we report a substrate S-acylation reconstitution assay, called the Pep-PAT assay, using purified enzyme and peptide fragments of substrates. We use the Pep-PAT assay to investigate the substrate S-acylation of three different zDHHC enzymes on seven different substrates. Remarkably, all the zDHHC enzymes showed robust activity with certain substrates but not others. These *in vitro* reconstitution experiments indicate that there is a preferred substrate hierarchy for zDHHC enzymes. We further used the Pep-PAT assay to interrogate the role of neighboring residues around the target cysteine on S-acylation of PSD-95 and SARS-CoV-2 Spike protein. Select residues around the target cysteines have distinct impact on substrate S-acylation, leading to the first insights into how neighboring residues around the target cysteine affect substrate S-acylation by zDHHC enzymes. Finally, we validated the impact of neighboring residues on substrate S-acylation using *in cellulo* assays. Our experiments build a framework for understanding substrate S-acylation by zDHHC enzymes.**

Decoration of proteins by attachment of lipids, collectively referred to as protein lipidation, is one of the most prevalent forms of protein modification, which occurs both co-translationally and post-translationally (1). Of these, protein S-acylation, commonly known as protein palmitoylation, is by far the most abundant with close to 6000 targets (2). Protein S-acylation results in the attachment of a long chain fatty acid, predominantly the 16-carbon palmitate, to cytosol-facing cysteines by a thioester linkage (3, 4) (Fig. 1*A*). Due to the increase in local hydrophobicity of modified proteins, S-acylation results in an augmented binding affinity to biological membranes (5). However, protein S-acylation can control numerous other aspects of protein function, including protein folding, stability, and interaction, some of which are just being discovered (6). Uniquely among all forms of protein lipidation, protein S-acylation is reversible and is thus a potentially dynamic modification (7) (Fig. 1*B*). Protein S-acylation intersects with myriad physiological processes such as signaling by small GTPases, localization of neuronal scaffolding proteins, and host–pathogen interactions. It has also been directly associated with numerous pathologies such as neurodegenerative diseases, neuropsychiatric diseases, and several forms of cancer (8, 9).

In humans, protein S-acylation is catalyzed by 23 members of the zDHHC family of integral membrane enzymes (10). zDHHC enzymes are characterized by a conserved Asp-His-His-Cys (DHHC) motif in their catalytic cysteine-rich domain (11, 12). There is considerable diversity in protein size, number of transmembrane helices, and the presence of conserved binding domains and motifs (5, 10). There is a much wider diversity in the substrates, which range from membrane to soluble proteins (1). Intriguingly, no consensus sequence is known for protein S-acylation, and *a posteriori* analysis suggests that membrane proximal cysteines have a higher propensity of being S-acylated. It is thought that zDHHC enzymes undergo an initial autoacylation, followed by a distinct transacylation step where the acyl group is transferred to the substrate (13). Despite having been discovered over 15 years ago (3, 4), there is very little understanding about how zDHHC enzymes interact with their substrates (5). Not only is there no understanding at the structural level about zDHHC–substrate interactions, but there is also very little understanding at the biochemical level as well. Most of the biochemical experiments have focused on a couple of zDHHC members with assays for autoacylation activity using a coupled enzyme assay (13). Although this assay reveals the activity of the enzyme for the first essential step using a small molecule thiol, *viz.* DTT, as a substrate, it is completely substrate agnostic and does not reflect the ability of the zDHHC enzyme to palmitoylate substrates at all.

With 23 zDHHC enzymes and approximately 6000 substrates, each zDHHC enzyme necessarily works on multiple

* For correspondence: Anirban Banerjee, anirban.banerjee@nih.gov.

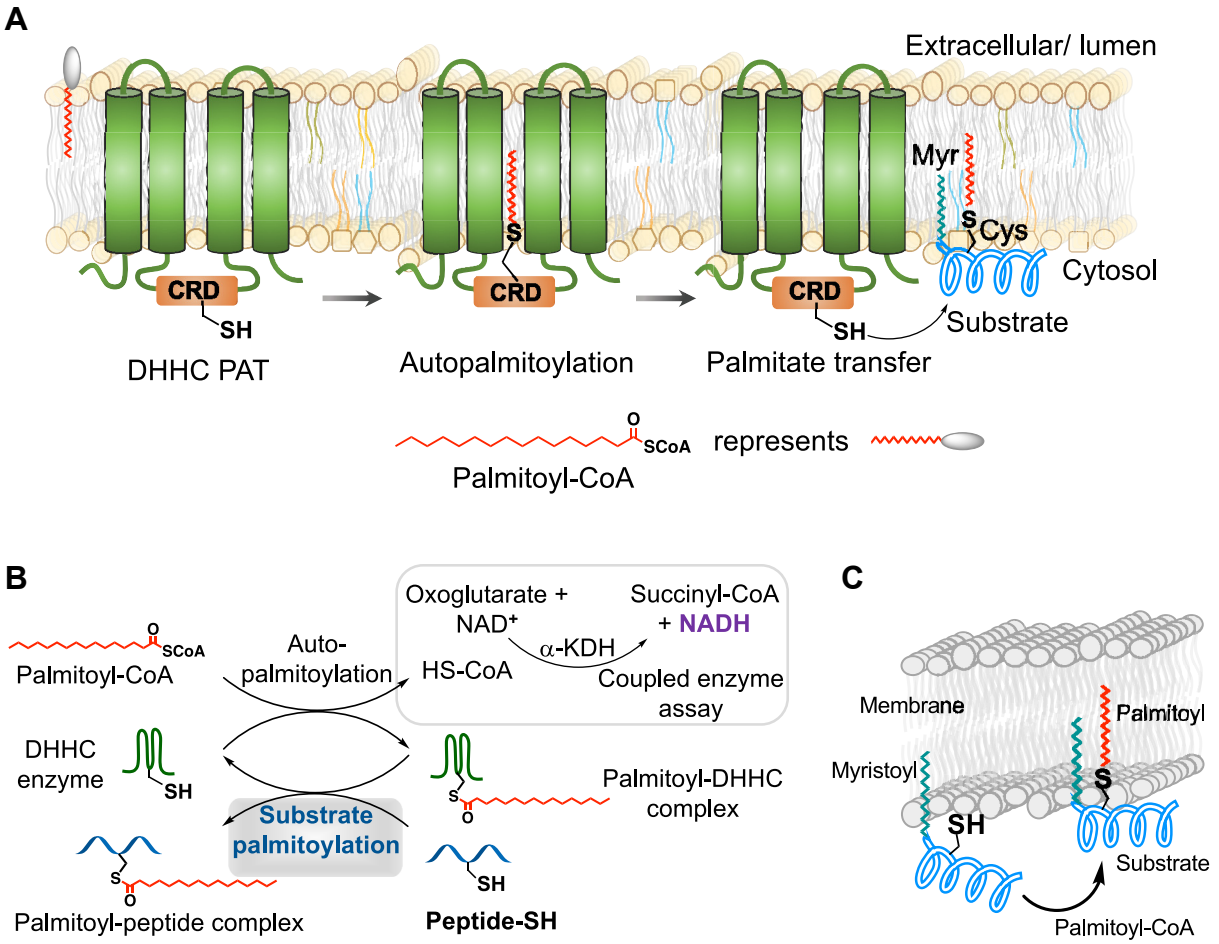


D

| Name of lipo-peptides | Sequences of the lipo-peptide substrates used | Origin of the lipo-peptides | zDHHC enzymes |
|---|---|---|---|
| SARS Pep | Myristoyl-G-MLCCMTSCCSCLKGCCSCGSCCKFDE-KG-$CONH_2$ | SARS-CoV2 Spike protein | zDHHC20 |
| GobX Pep | Myristoyl-G-QSRSCWSLFLYSIFGGKDNRK-KG-$CONH_2$ | GobX protein | zDHHC20 |
| EGFR1 Pep | Myristoyl-G-SNNSTVACIDRNGLQS-KG-$CONH_2$ | EGFR protein | zDHHC20 |
| EGFR2 Pep | Myristoyl-G-RNGLQSCPIKEDSFLQR-KG-$CONH_2$ | EGFR protein | zDHHC20 |
| PDL1 Pep | Myristoyl-G-KGRMMDVKKCGIQDTNS-KG-$CONH_2$ | PDL1 protein | zDHHC3 |
| $GABA_A$ Pep | Myristoyl-G-EYGYECLDGKDCASFFCCFED-K-G-$CONH_2$ | $GABA_A$ receptor | zDHHC3 |
| G11 α Pep | Myristoyl-G-MTLESMMACCLSDEVKESK-KG-$CONH_2$ | G11 α | zDHHC3 |
| PSD-95 Pep | Myristoyl-G-MDCLCIVTTKKYRYQ-KG-$CONH_2$ | PSD-95 | zDHHC15 |
| Control Peptide: without Myristoyl group, named as Non myristoylated- (NM-) Pep | | | |

**Figure 1. Design principle of Pep-PAT assay.** *A*, schematic showing reaction catalyzed by zDHHC enzymes. *B*, design of the Pep-PAT assay. A peptide fragment of the substrate is used as the surrogate substrate which makes it feasible to carry out the assay even for complex protein substrates. Every round of reaction generates free CoA, which is monitored using a coupled enzyme assay that generates fluorogenic NADH. *C*, illustration of the substrate in Pep-PAT assay with the N-terminal myristoyl modification to mimic the local hydrophobicity around target Cys. *D*, the sequence of the peptide substrates and the corresponding protein substrates used in the Pap-PAT assay in this work. For each peptide, an N-terminal Gly was added for appending the myristoyl modification and a C-terminal-LysGly sequence was added for solubility and ease of synthesis.

substrates. Yet, numerous cell-based experiments have revealed that many substrates can be S-acylated by multiple zDHHC enzymes (1). Thus, zDHHC–substrate interactions are not completely promiscuous, but there is overlapping substrate spectra between individual zDHHC enzymes. Problem with cell-based experiments is that the role of additional complex

factors cannot be eliminated. There are a vanishingly small number of examples of *in vitro* substrate S-acylation assays but these have either been carried out with qualitative assays with full-length proteins (11, 12, 14) or very small tripeptides (15) that do not capture adequately the footprint of the region around the target cysteines. This constitutes a large knowledge gap in the literature and has even led to doubts about whether there are any substrate–zDHHC interactions at all. This has been one of the most intriguing aspects of protein S-acylation. In the absence of robust *in vitro* reconstitution experiments, these questions about what, if at all, are the true determinants of substrate selectivity of zDHHC enzymes (16) have lingered in the field. Hence, there is a dire need for biochemical reconstitution experiments to study protein S-acylation for guiding hypotheses about zDHHC–substrate interactions. Here we develop a robust *in vitro* substrate S-acylation assay and use it to investigate the substrate S-acylation of three different zDHHC enzymes. We further use this assay to interrogate how neighboring residues affect S-acylation of two substrates, postsynaptic density protein-95 (PSD-95) and severe acute respiratory syndrome coronavirus 2 (SARS-CoV-2) Spike protein. We finally validate using *in cellulo* assays that mutation of neighboring residues indeed has a distinct impact on substrate S-acylation by zDHHC enzymes.

## Results

Our goal at the outset was to develop a fluorescence-based *in vitro* substrate S-acylation assay that could be widely adopted in different scenarios. Currently, the only *in vitro* assay for zDHHC enzymes that enables kinetic analysis is the coupled enzyme assay that only interrogates the first autoacylation step of zDHHC enzymes, is substrate agnostic, and couples the generation of free CoA to stoichiometrically equivalent NADH by using another enzyme, α-ketoglutarate dehydrogenase (α-KDH) (13). Typically, a small molecule thiol is used as a surrogate acceptor to regenerate the free enzyme. We replaced the small molecule thiol with a substrate peptide fragment containing the target cysteine (Fig. 1*B*). Since cysteines that are targets of S-acylation are typically proximal to the membrane, they are in a hydrophobic environment. To mimic the local hydrophobicity around the target cysteine, we appended an N-terminal myristoylation modification (Fig. 1, *C* and *D*) on the substrate peptide. To evaluate the validity of the N-terminal myristoylation appendage, we also synthesized non-myristoylated peptide substrates (Fig. 1*D*) and compared their activity with zDHHC enzymes.

We decided to focus on three different human zDHHC enzymes, human zDHHC3, 15 and 20. For substrate proteins, we used data from the literature that were obtained using *in vivo* or *in cellulo* experiments and selected a panel of proteins with the objective of having at least one established substrate for each zDHHC. Importantly, for each zDHHC, our panel of substrates also included several proteins that are known in the literature to be nonsubstrates. Our panel of substrate proteins include the following (Fig. 1*D*)—SARS-CoV-2 Spike protein (hereafter referred to as Spike) (17, 18), which interacts with the target host cells; GobX, an effector protein of the intracellular bacterial pathogen *Legionella pneumophila* (19); EGF receptor, a cell-surface signaling protein and a driver of tumorigenesis (20); programmed cell death ligand-1 (PDL1), an immune checkpoint inhibitor (21, 22); γ2 subunit of γ-aminobutyric acid type A ($GABA_A$) receptor (23, 24); α subunit of heterotrimeric $G_q$ protein (hereafter denoted as G11α) (25, 26); and PSD-95, a neuronal scaffolding protein (27).

### *A Pep-PAT assay for* in vitro *substrate S-acylation assay of zDHHC enzymes*

To demonstrate the proof-of-principle for the Pep-PAT assay, we performed pH-dependent substrate S-acylation (Fig. S1, *A–D*) using purified human zDHHC20 (hDHHC20) (12) and Spike as the substrate (Fig. 2*A*). The reaction progressed linearly within the range of pH 7.0 to 8.0 (Fig. S1, *B–D*), establishing the feasibility of our assay. hDHHC20 showed robust activity with Spike over background reaction. After calculating the ratio of initial velocity of hDHHC20 in the presence and absence of substrate peptide (Fig. S1*E*) as metric of activity, we decided to perform all the subsequent assays at pH 7.4 due to its relevance to physiological condition.

### In vitro *reconstitution of substrate discrimination by zDHHC20*

We then characterized S-acylation of Spike by hDHHC20 with the Pep-PAT assay in further detail. First, we checked the activity with varying concentrations of Spike ranging from 2 μM to 30 μM (Fig. S2, *A–F*) and determined the $K_m$ to be 5.42 ± 0.67 μM (Fig. 2*C*). Next, we performed the assay at six different concentrations of palmitoyl CoA (3 μM to 20 μM) (Fig. S3, *A–F*) and measured the $K_m$ to be 2.53 ± 0.23 μM (Fig. 2*D*). This is in close agreement with other measurements (12), strengthening the basis of the Pep-PAT assay. Encouraged by this, we evaluated two other substrates of zDHHC20—GobX and epidermal growth factor receptor 2 (EGFR2)—with the Pep-PAT assay. hDHHC20 showed robust activity with both substrates (Fig. 3*C* and Fig. S4, *A–B*). In sharp contrast, hDHHC20 showed very little activity with PSD-95, which has not been reported as a substrate of this particular zDHHC in literature (27), (Fig. 2*B*, Figs. 3*B*, and S7*A*). Similarly, hDHHC20 showed much less activity with PDL1, $GABA_A$, and G11α (Figs. 1*D*, 3*C* and S4*F*). Notably, *in cellulo* and *in vivo* experiments have shown all of them to be substrates of other members of the zDHHC family, but not zDHHC20. Finally, non-myristoylated substrates (Fig. S4, *C*–E, G) exhibited markedly diminished activity in comparison to the myristoylated substrates, thus validating our strategy of appending an N-terminal myristoyl linkage in the design of the substrates in the Pep-PAT assay. Thus, all our subsequent assays were conducted with an N-terminally myristoylated peptides.

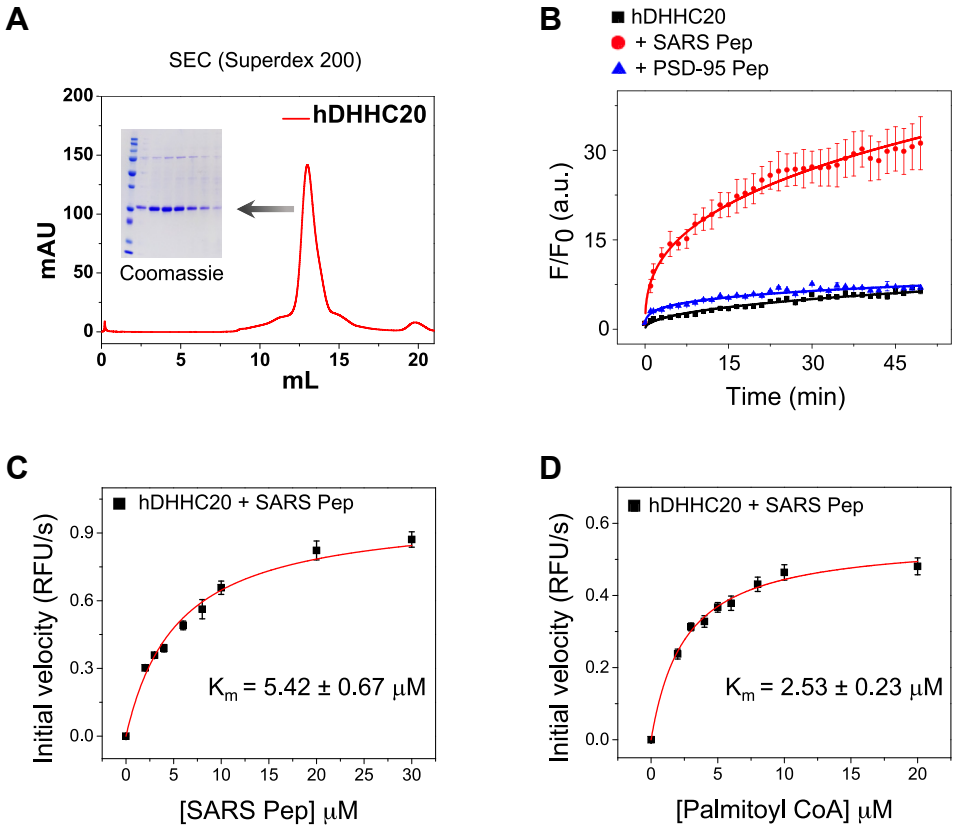


**Figure 2. Development of Pep-PAT assay.** *A*, size-exclusion chromatography of purified human zDHHC20 (hDHHC20) used for the assay. Inset shows the SDS-PAGE analysis of peak fractions. *B*, *in vitro* Pep-PAT assay using purified hDHHC20 (5 nm) and peptide fragments of SARS-CoV2 spike protein (10 μM) and PSD-95 protein (10 μM). The normalized fluorescence from NADH was plotted on the y-axis *versus* time on the x-axis. The different symbols indicate hDHHC20 with the different peptides as well the hDHHC-only control. SDs were calculated from multiple replicate measurements (n), where n = 3. The Michaelis–Menten constant ($K_m$) was determined from the Pep-PAT assay of hDHHC20 (5 nm) with variable concentrations of (*C*) SARS Pep substrate and (*D*) Palmitoyl CoA. The initial velocities of the individual curves (n = 3) were plotted on the y-axis to determine the kinetic parameters.

### *Dissection of substrate S-acylation of zDHHC3 and zDHHC15 enzymes with Pep-PAT assay*

Next, we turned our attention to interrogating substrate S-acylation by two other members of the family, zDHHC3 and zDHHC15, using the Pep-PAT assay. Intriguingly, PSD-95, that had earlier shown little activity with hDHHC20, displayed robust activity with human zDHHC15 (hDHHC15) (Fig. 3, *D* and *E*). PSD-95 is one of the most well-established substrates of zDHHC15 (27). In contrast, other substrates including Spike showed markedly less activity with zDHHC15 with the Pep-PAT assay (Figs. 3*E* and S5*B*). zDHHC15 has not been reported to be the palmitoylating enzyme for any of these substrates using *in cellulo* and *in vivo* experiments. Thus, the Pep-PAT assay recapitulates the essential aspects of substrate discrimination by zDHHC enzymes in the cellular environment.

zDHHC3 is one of the most active zDHHC enzymes with a wide range of substrates. human zDHHC3 (hDHHC3) showed robust activity with PDL1, $GABA_A$, and G11α with the Pep-PAT assay (Fig. 3, *F* and *G* and Fig. S6, *A*–*B*) while displaying much lower activity for Spike, GobX, and EGFR1 (Figs. 3*G* and S6*F*). Although zDHHC3 has not been shown to be one of the main palmitoylating enzymes for EGFR and PSD-95, zDHHC3 showed (Figs. 3*G* and S6*F*) higher activity with these substrates than hDHHC15 or hDHHC20 showed with nonsubstrates. We postulate that this is in accordance with the notion that zDHHC3 and zDHHC7 are more promiscuous members within the family that are less discerning towards select substrates (28).

### *Interrogate the role of the residues around the target cysteine on substrate S-acylation*

A critically understudied aspect of zDHHC enzymes is the determinants of the local environment of the target cysteine on substrate S-acylation. We therefore decided to use the Pep-PAT assay to examine the role of neighboring residues around target cysteine in the S-acylation of Spike by zDHHC20. We designed and synthesized a number of substrates (Fig. 4) with modified sequences mutating target cysteines as well as proximal residues. Mutating the first two Cys to Ala (Fig. 4*B*) diminished the activity considerably, as anticipated (Fig. 4, *B* and *C* and Fig. S8*A*). Mutation of other residues had varying degrees of effect on substrate S-acylation with the highest effect on SARS_mutant3 where the Met and Thr between the first and second Cys clusters in Spike were mutated to Ala (Fig. 4, *B* and *C* and Fig. S8, *C*–*E*). These results established the importance of specific residues around the target cysteines in the palmitoylation of Spike by zDHHC20.

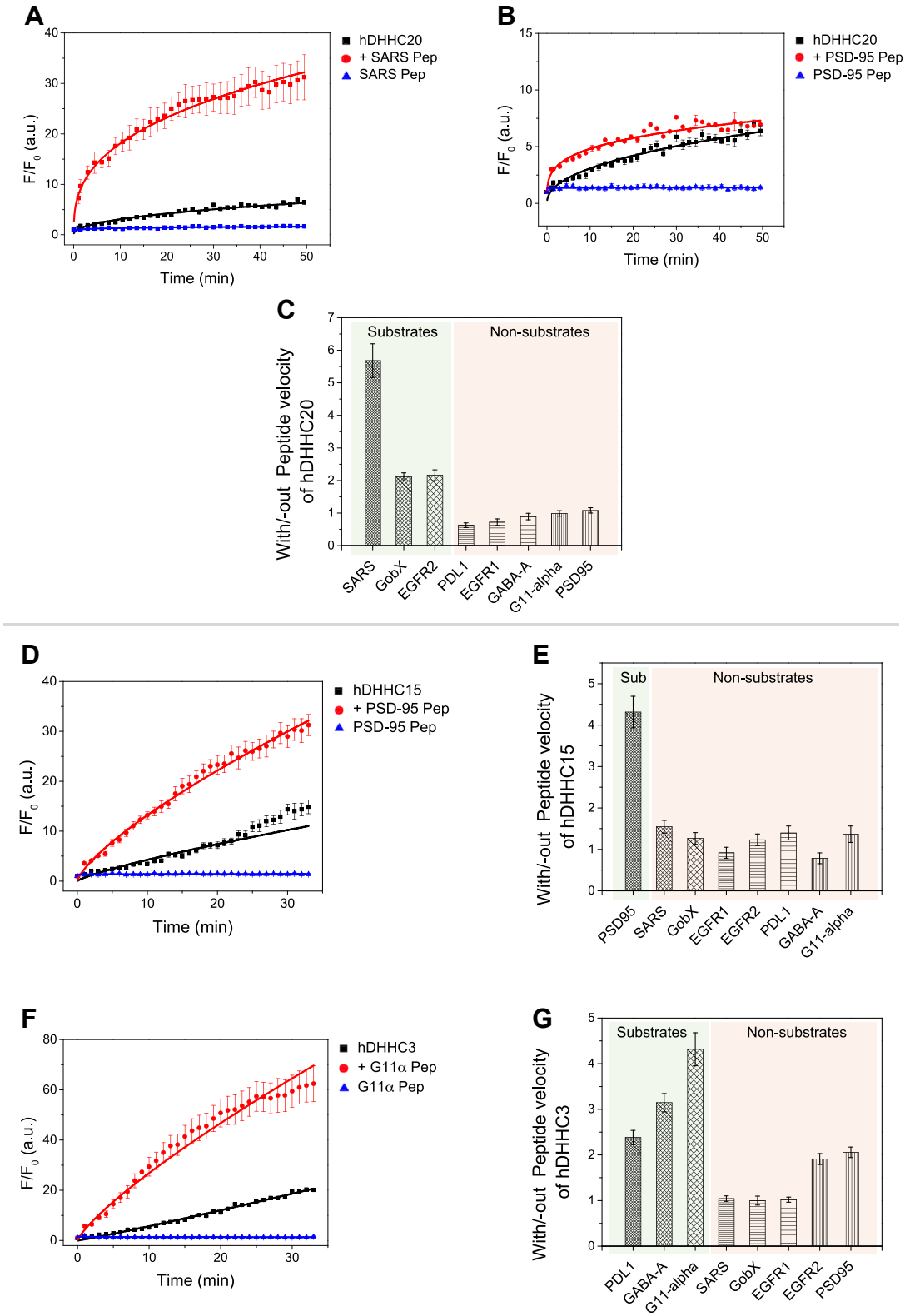


**Figure 3. Dissection of substrate S-acylation with Pep-PAT assay.** *A-C*, Pep-PAT assays, using purified hDHHC20 (5 nm) with (*A*) myristoylated (10 μM) SARS CoV-2 spike peptide and (*B*) myristoylated (10 μM) of PSD-95 peptide. Ten micromolar palmitoyl CoA was used to start the kinetics assays. The normalized fluorescence intensity from NADH was plotted on the y-axis and reaction timescale at the x-axis. Different symbols indicate the fluorescence of hDHHC20 in the absence and presence of peptide fragments and the peptides alone as control. SDs were calculated from multiple replicate measurements (n), where n = 3. *C*, for each substrate, the ratio of initial velocities of with and without the corresponding peptide is plotted on the y-axis. *D-E*, the Pep-PAT assays of purified hDHHC15 (25 nm) with (*D*) myristoylated PSD-95 substrate peptide (10 μM). The graphs were plotted as mentioned *vide supra*, where n = 4. *E*, for each substrate, the ratio of initial velocities of with and without the corresponding peptide is plotted on the y-axis. *F-G*, Pep-PAT assays of purified hDHHC3 (35 nm) with (*F*) myristoylated G11α substrate peptide (10 μM), where n = 5. *G*, for each substrate, the ratio of initial velocities of with and without the corresponding peptide is plotted on the y-axis. The statistical analyses have been included in supporting information (Table S4).

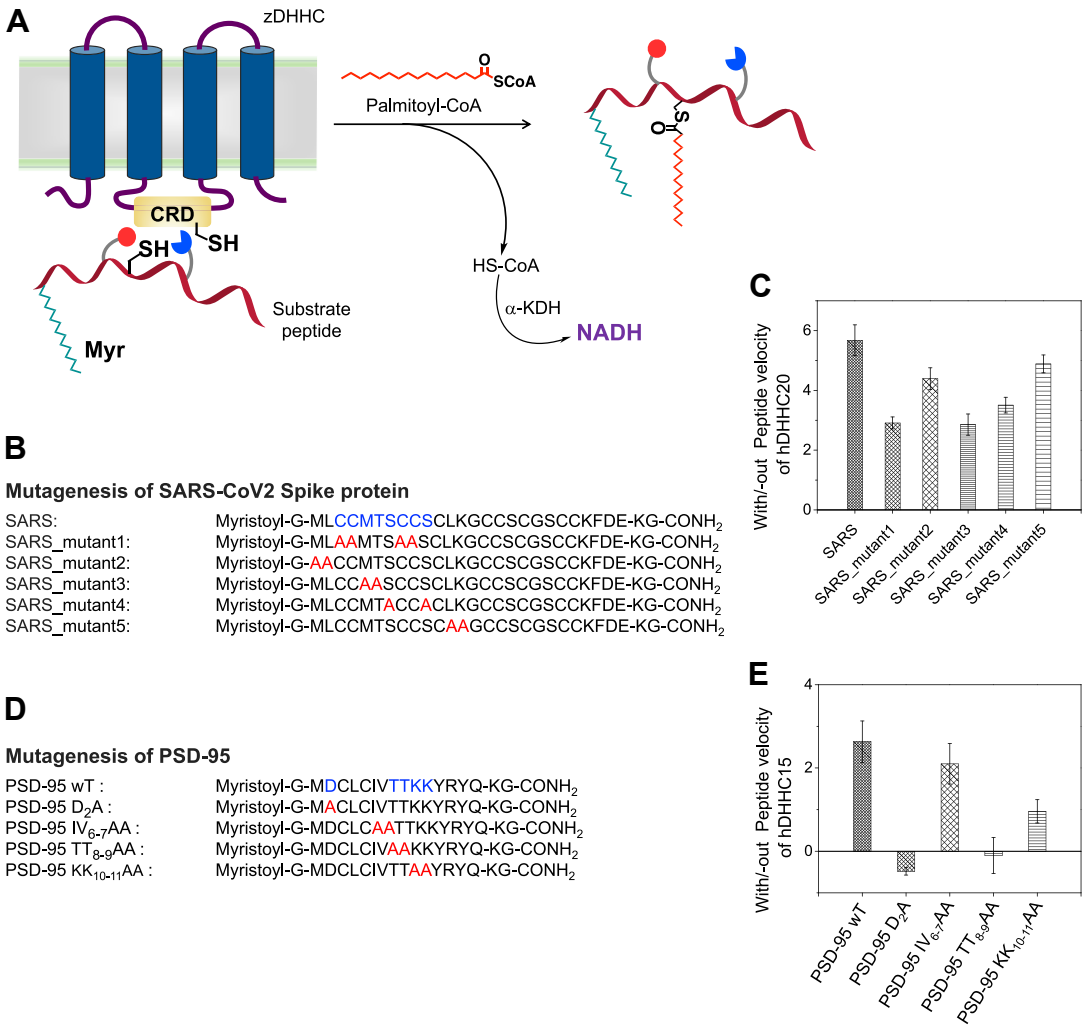


**Figure 4. Effect of neighboring residues on substrate palmitoylation.** *A*, schematic presentation of the role of residues nearby target cysteine on substrate palmitoylation. The sequences of the mutant peptides of (*B*) SARS-CoV2 Spike and (*D*) PSD-95 to study the effect of residues around target cysteine on substrate S-acylation. The Pep-PAT activity, quantified by the ratio of with and without peptide velocity of zDHHC, of the mutant peptides of (*C*) SARS-CoV2 Spike proteins and (*E*) PSD-95 proteins. The initial velocities were calculated from multiple replicate measurements (n), where n = 3. The statistical analyses have been included in the supporting information (Table S4).

We next focused on the effect of neighboring residues around the target cysteine on S-acylation of PSD-95 by hDHHC15. We synthesized four mutants (Fig. 4*D*) of PSD-95 replacing residues with distinct physico-chemical characteristics, by Ala, and examined their activities with hDHHC15 using the Pep-PAT assay. Mutants of PSD-95 showed much more dramatic effects on palmitoylation by hDHHC15. Mutation of a single acidic residue, Asp2, by Ala, resulted in negligible S-acylation (Fig. 4, *D* and *E* and Fig. S9*A*). Similarly, mutation of Thr8 and Thr9 resulted in a similar loss of S-acylation (Fig. 4, *D* and *E* and Fig. S9*C*). Intriguingly, concurrent mutation of two hydrophobic residues, Ile6 and Val7, to Ala, that are adjacent to one of the target cysteines, Cys5, had a much less effect on S-acylation compared to mutating Thr8 and Thr9, suggesting that the effect is not mere loss of hydrophobic side chains but more specific (Figu. 4, *D* and *E* and Fig. S9, *B*–*C*). Double mutation of two positively charged Lys residues, Lys10 and Lys11 (Fig. 4, *D* and *E* and Fig. S9*D*), was more prominent than the Ile6Ala/Val7Ala mutant but less drastic than Thr8Ala/Thr9Ala double mutant.

### *Pep-PAT assay in nanodiscs to interrogate the effect of neighboring residues on PSD-95 S-acylation by zDHHC15*

The Pep-PAT assays presented thus far have been carried out with detergent solubilized enzymes. Lipid nanodiscs (29) are better mimetics of the native environment of membrane proteins and thus, we next decided to investigate the activity of zDHHC enzymes in nanodiscs (30) using the Pep-PAT assay. The advantage of nanodiscs is that it enables controlling the lipid composition of the disc. We purified the zebrafish homolog of zDHHC15, reconstituted in POPC nanodiscs, which showed robust activity with PSD-95 (Figs. S10 and Fig. 5, *A*–*C*). When we investigated the activity of the different mutants of PSD-95 with nanodisc-reconstituted zDHHC15, the Asp2Ala and the Thr8Ala/Thr9Ala double mutants showed

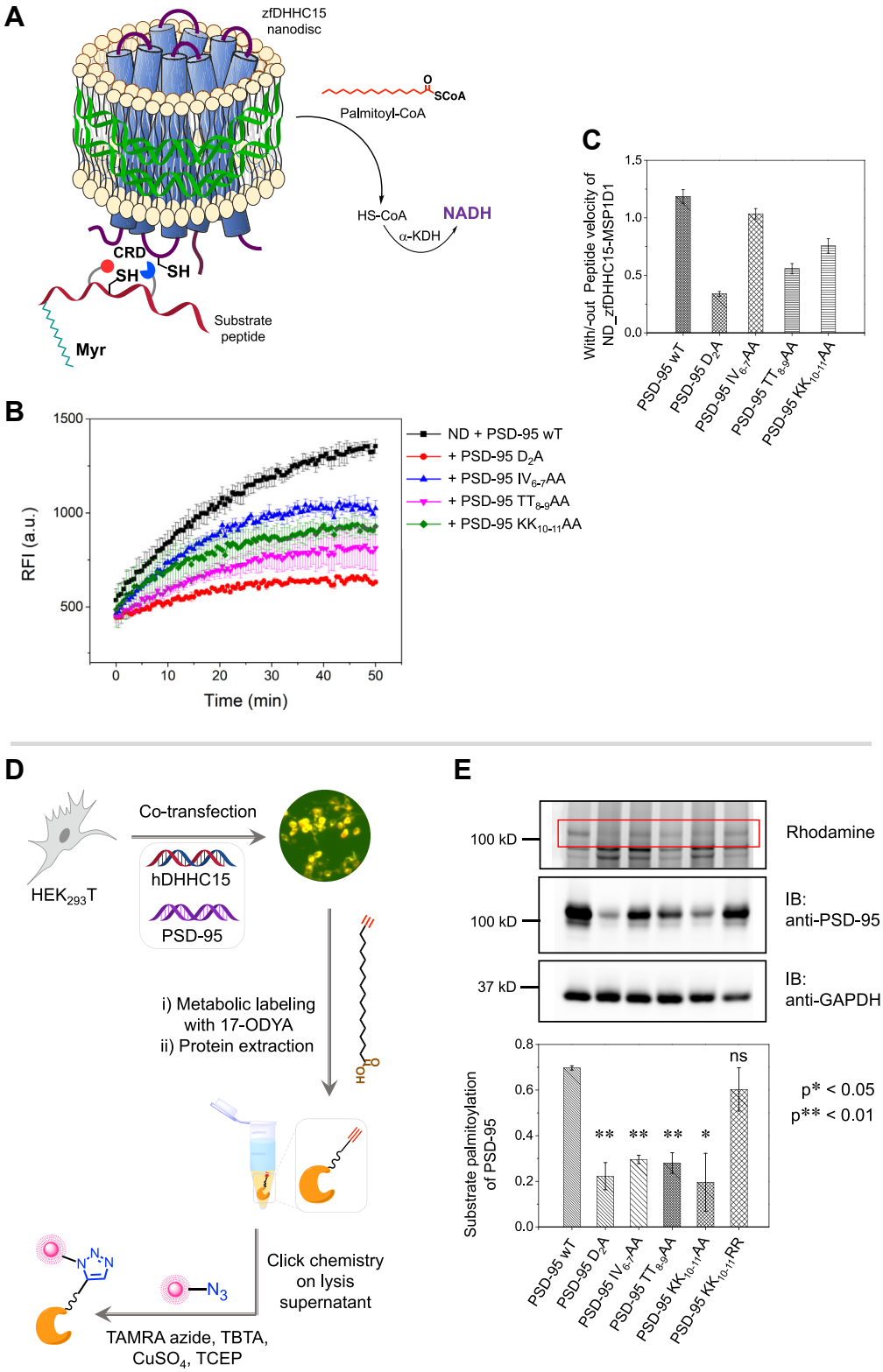


**Figure 5. Pep-PAT assay in nanodiscs and *in cellulo* substrate S-acylation.** *A*, schematic diagram of the Pep-PAT assay with the zDHHC enzyme reconstituted in lipid nanodiscs. Neighboring residues around the target cysteine are represented with *red* and *blue spheres*. *B*, *in vitro* assay using purified zebrafish zDHHC15 (zfDHHC15) nanodiscs (25 nm, reconstituted with POPC) and PSD-95 peptide (10 μM) and its mutants. The relative fluorescence intensity (RFI), calculated from the fluorescence intensity of NADH over background acylation, was plotted on the y-axis alongside reaction timescale at the x-axis. The different symbols signify the RFI of zfDHHC15 nanodisc along with mutants. SD were calculated from multiple replicate measurements (n), where n = 4. *C*, for each mutant, the ratio of initial velocities of with and without the corresponding peptide is plotted on the y-axis. *D*, the workflow for *in cellulo* substrate palmitoylation of PSD-95 against hDHHC15. *E*, the quantification of PSD-95 substrate palmitoylation by dividing the intensity of its band in the rhodamine detection gel (*top*) by anti-PSD-95 immunoblot (*middle*) signal. *$p < 0.05$, **$p < 0.01$.

the most disruption in activity followed by Lys10Ala/Lys11Ala double mutant. The Ile6Ala/Val7Ala double mutant showed the least impact on palmitoylation activity (Fig. 5, *B* and *C*). Thus, the experiments with nanodisc-reconstituted zDHHC15 reinforce the importance of Asp2, Thr8, and Thr9 of PSD-95 in S-acylation by zDHHC15.

We further investigated the effect of the mutations on PSD-95 S-acylation by hDHHC15 using *in cellulo* click chemistry–based experiments. These showed a similar effect of the Asp2Ala and the Thr8Ala/Thr9Ala double mutant on PSD-95 palmitoylation (Fig. 5, *D* and *E*). Notably *in cellulo* experiments revealed a more prominent effect of the Ile6Ala/Val7Ala as well as the Lys10Ala/Lys11Ala double mutants (Fig. 5*E*). We tested an additional double mutant in the *in cellulo* experiments where Lys10 and Lys11 were mutated to Arginine (Fig. 5*E*). This mutant regained its activity, comparable to wild-type PSD-95 suggesting an electrostatic contribution of the lysine residues, which is lost in the double alanine mutant but is presumably regained in the double arginine mutant.

## Discussion

With ∼6000 palmitoylated proteins and 23 zDHHC enzymes, a complex enzyme–substrate interaction network underlies protein S-acylation. Yet, this has been largely uncharacterized except the interaction between zDHHC13 and zDHHC17 and their substrates that occurs through well-defined substrate interaction domains (31). We posit that the most severe bottleneck towards a comprehensive understanding of substrate interactions of zDHHC enzymes is the lack of a robust *in vitro* substrate S-acylation assay with purified components. Moreover, *in cellulo* experiments indicate that many substrates can be S-acylated by more than one zDHHC enzymes raising the question whether there are any zDHHC–substrate interactions at all. It is difficult to address this question using only *in cellulo* experiments given that the contributions of many complicating factors cannot be delineated. Here we report the development of a robust *in vitro* substrate S-acylation assay, that we call the Pep-PAT assay, using purified zDHHC enzymes. Since there are many complex substrate proteins including transmembrane proteins, we establish our assay using peptide fragments of substrates that make it amenable for using this assay to understand the S-acylation of any substrate. Our assay is also amenable for analyzing the kinetics of substrate S-acylation, a distinct advantage over other *in vitro* assays (Table S3). We demonstrate the robustness of this assay with three different zDHHC enzymes and seven different substrate proteins ranging from small soluble proteins to multipass transmembrane cell surface receptors.

Our results indicate clear difference in the activity of zDHHC enzymes for different substrate proteins. These results agree remarkably well with data from the literature with *in cellulo* experiments that have established the candidate zDHHC enzymes for each of these substrates. This argues that at least for the three zDHHC enzymes in this study, there are preferred substrates, which in turn suggest substrate selective interactions at the zDHHC–substrate interface. The close agreement of our results and data from the literature also reinforce the design of our substrates and that the essential aspects of the *in cellulo* reaction is captured in our *in vitro* Pep-PAT assay. To our knowledge, this is the first *in vitro* reconstitution and demonstration of substrate selectivity of zDHHC enzymes using the same panel of substrates and multiple zDHHC enzymes.

Yet another poorly understood aspect about S-acylation is how residues around the target cysteine affect substrate S-acylation by zDHHC enzymes. We use the Pep-PAT assay and two different substrates, SARS-CoV-2 Spike protein and PSD-95, to demonstrate that specific residues around the target cysteines have much more impact on substrate S-acylation than other residues, thus arguing for them to be important at the protein–protein interface during substrate S-acylation. We further establish the Pep-PAT assay in lipid nanodiscs to interrogate the effects of the surrounding residues on substrate S-acylation assay in a more native membrane-like environment. To our knowledge, this is the first demonstration of substrate S-acylation by zDHHC enzymes in a nanodisc reconstituted format. Our results in lipid nanodiscs agree remarkably well with the results from Pep-PAT assay in detergent micelles. Finally, we corroborate our results from *in vitro* assays with *in cellulo* experiments with full-length substrate, PSD-95, and click chemistry, which strengthen our conclusions from Pep-PAT assay in detergents and nanodiscs. zDHHC enzymes are localized in distinct compartmental membranes with specific lipid composition. This assay will further enable the investigation of zDHHC enzymes in specific lipid composition and connect them to their native cellular environment.

There are no consensus sequences known for protein S-acylation and the only aspect that has been recognized is that cysteines targeted for S-acylation are membrane proximal. zDHHC enzymes are transmembrane enzymes, and long chain fatty acyl CoAs are amphipathic substrates that may already reside in the membrane (32). Thus, it is quite likely that the interaction between zDHHC enzymes and substrates may involve membrane lipids as part of a supramolecular complex. However, in order to dissect the interactions between zDHHC enzymes and their substrates, it is critical to understand each of these components separately. An *in vitro* S-acylation assay opens up ways to exactly achieve that. We show using the Pep-PAT assay that zDHHC3, zDHHC15, and zDHHC20 enzymes have distinct preferences for certain substrates over others. Thus, within the context of the sequences around the target cysteines captured in our substrate fragments, there is sufficient potential to discriminate between different zDHHC–substrate interactions. It is quite likely that the full-length substrates have additional interactions. Similarly, there are likely interactions engaged by the membrane lipids at the zDHHC–substrate interface. Our nanodisc-reconstituted Pep-PAT assay now opens up ways to investigate this aspect for discrete zDHHC–substrate pairs. Further structural and biochemical experiments combined with chemical biology, and cell biological approaches will be required to appreciate the full atomic complexity of zDHHC–substrate interactions that underlie the physiology of protein S-acylation.

## Experimental procedures

### Molecular biology

The expression constructs for human zDHHC3 and human zDHHC15 were generated by inserting the protein coding sequence into a modified BacMam vector with N-terminal decahistidine and an mVenus tag (33), whereas the expression construct for PSD-95 was generated by modifying BacMam vector with C-terminal mCherry and a decahistidine tag (33).

### Procedure of lipo-peptide synthesis, purification, and characterization

All the lipo-peptides were synthesized by standard Fmoc/$^{t}$Bu solid phase peptide synthesis method (34, 35) using microwave-assisted CEM Liberty PRIME peptide synthesizer. Briefly, the Fmoc group attached with the Rink amide AM resin (loading 0.45 mmol/g) was cleaved with 20% piperidine in N,N-dimethylformamide (DMF), followed by coupling with 3.0 equivalent of Fmoc amino acid, 4.0 equivalent of HBTU (coupling reagent), and 5.5 equivalent of N,N-Diisopropylethylamine (DIPEA, base). It was then acetylated (capping) to block unreacted amine with 2.0 equivalent of acetic anhydride and N-methyl imidazole in DCM and considered it as the preloaded resin. The cycle of the cleavage of Fmoc group of terminal amino acid and coupling of desired amino acids were continued on CEM peptide synthesizer using 25% piperidine, 0.25 M Oxyma pure, and 0.25 M DIC along with 0.06 M DIPEA in DMF solvent. The N-terminus myristoyl modification was carried out by coupling with 4.0 equivalent of myristic acid, 5.0 equivalent of HBTU, and 8.0 equivalent of DIPEA in DMF. Finally, the C terminus of the lipo-peptide was cleaved from the Rink amide resin with a mixture of TFA: Triisopropylsilane: DCM (8.5: 0.5: 1.0) for 3h (or 5h where necessary). Reagent K [TFA: phenol: water: thioanisole: 1,2-ethanedithiol (82.5: 5.0: 5.0: 5.0: 2.5)] was used for multiple Cys (>8, Trt protected) containing lipo-peptide to cleave it from resin, while a cocktail of TFA: 1,2-ethanedithiol: DCM (97: 2.5: 0.5) was applied for lipo-peptide having <7 Cys.

The reaction mixture was subsequently precipitated by cold diethyl ether to get the crude lipo-peptide that was dissolved in $CH_3CN/H_2O$. Purity of the lipo-peptides was confirmed using UFLC SHIMADZU analytical system. A Vydac 218TP 5 μM C4 analytical column, flow rate of 0.8 ml/min, linear gradient of 5 to 75 to 95% $CH_3CN$ for 5-10 to 25 min, over a total run time of 32 min were used. Binary solvent system [solvent A (0.1% TFA in $H_2O$) and solvent B (0.1% TFA in $CH_3CN$)] and RF-20A detector with dual detection at 214 and 254 nm were used.

The mass spectral data was obtained using a Waters qTOF instrument (Model Xevo G2) with the ionization mode of electrospray positive ion and ESI capillary voltage of 2.8 KV. Samples were injected onto a ProSwift RP-4H 1 × 50 mm column with a flow rate of 0.250 ml/min in a binary solvent system (solvent A was $H_2O$ with 0.2% FA and solvent B was 100% ACN with 0.2% FA and 0.1% TFA added). The elution profile was 100% solvent A at time 0 and then solvent B was increased to 60% in 3 min and held for 3 min. The data was collected and analyzed using the Water Mass Lynx 4 software package.

### Yeast transformation

Expression of plasmid linearization, competent yeast preparation, and yeast transformation were carried out using standard methods and the transformants were selected on YPDS plates containing ∼400 μg/ml zeocin.

### Protein expression and purification

#### Yeast cell culture and lysis

Large-scale yeast culture, induction of protein expression, and cell lysis were executed as reported previously (36). Concisely, 300 ml BMG (0.1 M potassium phosphate, pH 6.0, 3.4 g/L yeast nitrogen base, 1% glycerol, 0.4 μg/ml biotin) with 400 μg/ml Zeocin cultures of yeast were grown for ∼24h at 30 °C with vigorous shaking at 240 rpm. Approximately, eighty milliliters of the sample cultures, that generally reached cell densities of $A_{600}$ ∼20, were inoculated to 1.5 L cultures in the same media excluding Zeocin for ∼36h at 30 °C, 240 rpm. The cells were then pelleted by centrifugation at 3500*g*, 4 °C for 15 min and washed methodically with BMM (0.1 M potassium phosphate, pH 6.0, 3.4 g/L yeast nitrogen base, 1% methanol, 0.4 μg/ml biotin). The cells were resuspended in 1.5 L of BMM media and protein expression was induced at 24 °C for 24h. Cells were harvested by centrifugation at 3500*g*, 4 °C for 20 min. Finally, the harvested cell pellets were flash-frozen in liquid $N_2$ and stored at −80 °C. Cells were lysed by cryo-milling using Retsch MM400 Millers with liquid $N_2$.

#### Purification of hDHHC20

The purification of hDHHC20 was carried out as described previously (12). Briefly, ∼10 g of cryo-milled cell powder was suspended in 100 ml of lysis buffer containing 100 mM Hepes of pH 7.5, 450 mM NaCl, 1.25% (w/v) n-dodecyl-β-D-maltopyranoside (DDM), 5 mM β-Mercaptoethanol (βME), 1X protease inhibitors [pepstatin, leupeptin, soy trypsin inhibitor, aprotinin, benzamidine, 4-(2-aminoethyl)- benzenesulfonyl fluoride hydrochloride (AEBSF), PMSF, and deoxyribonuclease (DNase)]. The lysate was extracted using a magnetic stirrer for 3h at 4 °C and centrifuged afterward at 38,000 g for 30 min at 4 °C. The supernatant was mixed with 1 ml of TALON metal affinity resin, rotated for 2h at 4 °C, and then loaded onto a Bio-Rad Econo column. The column was washed with five column volumes of wash buffer containing 50 mM Hepes of pH 7.6 (finally adjusted), 250 mM NaCl, 2 mM tris(2- carboxyethyl)phosphine (TCEP), and 2 mM DDM along with 10 mM and 20 mM of imidazole successively; followed by an additional wash with five column volumes of the similar buffer excluding imidazole. Next, the protein-bound resin was resuspended in two column volumes of wash buffer (excluding imidazole) prior to on-column PreScission protease cleavage. The resin slurry was then allowed to rotate overnight at 4 °C. The cleaved protein was collected by gravity flow and concentrated with a 30 kD molecular weight cut-off (MWCO) concentrator to 0.5 ml. The concentrated protein was loaded onto a Superdex 200 size-exclusion column equilibrated with buffer consisting of 20 mM Hepes of pH 7.5 (finally adjusted), 150 mM NaCl, 2 mM TCEP, and 0.5 mM DDM at 4 °C.

Finally, the targeted fractions of the protein were pooled and concentrated using the similar concentrator.

*Mammalian cell culture*

Human embryonic kidney cells 293T (HEK293T) ATCC CRL-3216 were cultured in Dulbecco's modified Eagle's medium (DMEM) without glutamine supplemented with 10% fetal bovine serum, L-glutamine, and penicillin-streptomycin. Cells were propagated with 5% $CO_2$ and humidity at 37 °C. Transfection was performed at 70 to 80% confluency of HEK293T cells in a 10 cm tissue culture dish. Purified DNA (in elution buffer, AE) and polyethylenimine (PEI, dissolved in PBS at 1 mg/ml and readjusted to pH 7.0) were diluted in unsupplemented DMEM followed by mixing them at a ratio of 1:3 and incubated for ∼20 min at room temperature. Subsequently, the DNA–PEI mixture was added to the cells dropwise and incubated at 37 °C in a $CO_2$ incubator for ∼36h post transfection before harvesting the cells.

*Expression and purification of hDHHC15 and hDHHC3 enzymes*

pBacmam_hDHHC15_cGFP and pBacmam_hDHHC3_cGFP were expressed in HEK293T cells passaged in 10 cm tissue culture dish as portrayed in "mammalian cell culture" *vide supra*. Cells were transfected using 10 μg of DNA with three-fold molar excess of PEI following harvested the cells after ∼36 h, then washed with 1X PBS before flash freezing in liquid nitrogen, and stored at −80 °C. Frozen cells were thawed on ice, resuspended in 600 μl of lysis buffer containing 50 mM Tris, pH 7.5, 200 mM NaCl, 5 mM βME, 2% DDM, and protease inhibitors (pepstatin, leupeptin, soy trypsin inhibitor, aprotinin, benzamidine, AEBSF, PMSF, and DNase), and allowed to rotate for ∼3h at 4 °C. Post extraction, the lysate was centrifuged at 20,000 g, 4 °C for 20 min. Then, 150 μl of pre-equilibrated TALON resin was resuspended with the supernatant and mixed on a rotator for ∼2h at 4 °C. The resin slurry was spun down at 800 g for 10 min at 4 °C. Subsequently the resin was washed first with talon buffer comprising of lysis buffer and 0.1% DDM, then with 30 mM imidazole containing talon buffer, and finally with talon buffer to remove imidazole. The protein-bound resin was eluted in 350 μl of elution buffer having lysis buffer with 0.1% DDM and PreScission protease. The cleaved protein was collected by centrifuging at 800 g, 4 °C for 10 min and concentrated down using a 30 kD MWCO centrifugal filter to 1 μM to use immediately for *in vitro* assay.

*In vitro reconstitution of Pep-PAT assay*

The Pep-PAT assay was developed by modifying fluorescence-based coupled-enzyme assay (12, 13) in 96-well format at 30 °C. Plates were read in a Tecan M1000Pro plate reader with excitation wavelength at 340 nm (bandwith of 5 nm) and emission wavelength at 465 nm (bandwith of 10 nm). The final reaction volume (60 μl) contained 0.25 mM oxidized nicotinamide adenine dinucleotide ($NAD^+$), 0.2 mM thiamine pyrophosphate, 2 mM 2-oxoglutarate, 0.2 mM DDM in 50 mM Hepes buffer at pH 7.4, and 50 mM NaCl. The kinetic assays were initiated by the addition of 10 μM palmitoyl-CoA and monitored up to 50 min in the case of hDHHC20 and 35 min for hDHHC15 and hDHHC3 at 30 °C. We prepared the αKDH in-house from beef heart using published protocol (37). The DHHC enzyme concentrations in the assay was 5 nM for hDHHC20, 25 nM for hDHHC15 (10 nM for mutagenesis), and 35 nM for hDHHC3 to determine kinetic parameters. The lipo-peptide substrates of 10 μM were added to the reaction mixture prior to the addition of palmitoyl-CoA. All the parameters were optimized by considering a wide range of substrates and non-substrates against different zDHHC enzymes to determine the initial velocity comparatively. The fluorescence intensity of produced NADH (F) was divided by that of background acylation ($F_0$) before calculating the initial velocity. $K_m$ was determined from the Michaelis–Menten equation using nonlinear fittings in OriginLab Pro8.5. The nonlinear curve-fitting was weighted to the error and repeatedly performed to minimize reduced chi-square. Adjusted r-square values obtained were >0.95 for most of the fits. SDs were calculated from multiple replicate measurements.

### Reconstitution of nanodiscs

*Expression and purification of MSP1D1 and zfDHHC15*

The MSP1D1 was expressed and purified as described previously (38). In short, after transforming DNA into BL21 cells, a single colony of MSP1D1 was inoculated with 50 ml LB media along with 50 μl kanamycin (50 mg/ml) and grown for overnight at 37 °C. The obtained inoculum (∼10 ml, A ∼0.1) was added into 1 L of Terrific broth with $KP_i$ and kanamycin to grow for ∼2.5 h (A ∼0.5), then induced by IPTG and grown for another ∼5h post induction. The cells were pelleted by centrifuging at 6000 g for 15 min at 4 °C and stored at −80 °C. For purification, ∼10 gm of frozen cells was added to 50 ml of lysis buffer containing 2X PBS of pH 8.0, 1% Triton X-100, 1 mM PMSF, 1X AEBSF, 5 mM βME, and DNAse and allowed to stir for 30 min at 4 °C followed by appropriate sonication and consequent centrifugation at 38,000 g for 30 min, 4 °C. The supernatant (pH 7.4) was bound to 2 ml of TALON metal affinity resin and then washed with 40 mM Tris–HCl (pH 8.0) and 400 mM NaCl that was supplemented with 1% Triton X-100 (wash 1, 10 bed volume), 50 mM sodium-cholate (wash 2), and 30 mM imidazole along with 5 mM βME (wash 3). The protein-bound resin was eluted with wash buffer having PreScission protease and 1 mM βME for overnight at 4 °C. The flow-through was concentrated using 10 kD MWCO concentrator and purified by size-exclusion chromatography (SEC) onto a Superdex 200 column in 1X TBS of pH 7.4.

The expression and purification of zfDHHC15 from Pichia were performed as mentioned before (12). In brief, frozen cell powder was suspended in lysis buffer (∼12 g of cell in 75 ml lysis buffer) containing 50 mM Tris–HCl of pH 7.5, 150 mM NaCl, 1 mM TCEP, and 1X protease inhibitors followed by the addition of 1.2 gm of DDM after adjusting the pH of the lysate to 7.8. The proteins were extracted by

stirring the cell lysate for 3h at 4 °C, subsequently adjusted the pH to 7.5, and centrifuged at 38,000 g for 30 min at 4 °C. The supernatant was mixed with 2 ml of TALON metal affinity resin pre-equilibrated with lysis buffer supplemented with 1 mM DDM, rotated for 3h at 4 °C, and then collected in a Bio-Rad Econo column. The column was washed with 10 bed volumes of wash buffer 1 containing 20 mM Tris–HCl of pH 7.5, 150 mM NaCl, 1 mM TCEP, and 2 mM DDM, then with wash buffer 2 containing 20 mM of imidazole along with wash buffer 1, followed by an additional wash with wash buffer 1 to remove imidazole. The protein-bound resin was resuspended in wash buffer 1 supplemented with PreScission protease to cleave N-terminus His10 tagged GFP by rotating overnight at 4 °C. The flow-through containing cleaved protein was concentrated with a 50 kD molecular weight cut-off concentrator to 0.5 ml and purified by SEC onto a Superdex 200 column in buffer having same composition as wash buffer 1. The peak fractions of the protein were pooled and concentrated using 50 kD MWCO concentrator.

#### *Reconstitution of zfDHHC15 nanodiscs in POPC lipid*

Before starting the reconstitution, ∼1 gm of bio-beads was washed with MeOH and left overnight to activate it followed by washing with mQ water and 1X TBS. A 50 mM stock of sodium cholate in 1X TBS was prepared. POPC (25 mg/ml in chloroform) was dried separately to a film by purging argon followed by vacuum desiccator and dissolved in 1X TBS with 50 mM of sodium cholate by repeated sonication and dipping in 42 °C water bath to make a 10 mM of lipid-stock solutions. The zfDHHC15 nanodiscs reconstitutions were performed in the following condition: 18.75 μM of zfDHHC15, 37.5 μM of MSP1D1, and 3.0 mM of POPC in a final concentration of 15 mM sodium cholate in 1X TBS (pH 7.4) at 4 °C. At first, the cholate-solubilized lipids were added to MSP1D1 in 1X TBS at 4 °C and allowed the reaction mixture to settle for 30 min followed by the addition of concentrated zfDHHC15. The reaction mixture was rotated gently for 2 h at 4 °C and then ∼0.1 g of prepared bio-beads was added to the mixture followed by another addition of ∼0.4 g of bio-beads after 2 h of interval and left overnight. After that, the solution was separated from bio-beads and concentrated using 50 kD MWCO concentrator and purified by SEC onto a Superdex 200 column in 1X TBS of pH 7.4 along with 1 mM TCEP. The desired fragments of the nanodiscs were collected and concentrated down using a 50 kD MWCO concentrator to use for *in vitro* assay.

#### *In vitro reconstitution of Pep-PAT assay with nanodiscs*

The buffer composition of the Pep-PAT assay was modified to perform the assay in the presence of nanodiscs. The detergent DDM was excluded from the reaction. The final reaction volume (60 μl) contained 30 μM palmitoyl-CoA, additional 1 mM TCEP in 50 mM Hepes buffer of pH 7.4, and 150 mM NaCl having rest of the components *vide supra* remain unaltered. The zfDHHC15 nanodiscs concentrations in the assay were 25 nM. The lipo-peptide substrates were added at the end to start the kinetics. The relative fluorescence intensity (RFI) of produced NADH was presented after normalization in terms of background acylation before calculating the initial velocity. SDs were calculated from at least five replicate measurements.

#### *Substrate palmitoylation in cellulo*

Single point mutation of PSD-95 mutants was generated using site-directed mutagenesis protocol. All clones were confirmed by DNA sequencing. HEK293T cells were cultured and cotransfected with hDHHC15 and PSD-95 mutants in a 1:2 ratio as described *vide supra*. A 10 cm tissue culture dishes were used to prepare the cells for the assay. After ∼36 h of cotransfection, the growth medium was replaced with 10 ml of DMEM supplemented with 5% dialyzed FBS containing 17-octadecynoic acid (10 μl of 100 mM stock). The cells were incubated for 6 h which was harvested and kept at −80 °C after flash freezing. Consequently, the cells were lysed in 200 μl of detergent-containing buffer (as described in the purification procedure) followed by performing click-chemistry reaction (using standard protocol) containing TAMRA azide (Lumiprobe), Tris[(1-benzyl-1H- 1,2,3-triazol-4-yl)methyl]amine, freshly prepared CuSO4, and TCEP, which were then added to the lysis supernatant and incubated for 1 h at 30 °C with intermittent mixing under dark condition. Proteins were then added to 4X SDS-sample buffer with 20% βME and allowed to rotate for mixing. Eight microliters of individual sample were loaded onto 4 to 20% SDS-Page gel which was visualized by a ChemiDoc System (BioRad). After detecting the Rhodamine-labeled proteins using Rhodamine channel, the gel was then transferred to polyvinylidene difluoride membrane followed by incubation with blocking buffer. Next, the portion of membrane corresponding to PSD-95 was incubated with anti-PSD-95 antibody (Thermo Fisher Scientific), while another portion of the membrane was incubated with anti-GAPDH antibody (Thermo Fisher Scientific) for overnight at 4 °C with mild agitation. Membranes were washed three times with wash buffer and incubated with anti-mouse secondary antibody (Thermo Fisher Scientific) for 1 h with mild agitation. Then the membranes were developed using Super Signal West Femto Reagents and imaged on a Chemidoc (Bio-Rad). The quantitation of protein bands was achieved by Fiji (ImageJ) software.

## Data availability

All data and results are available upon request from the authors and are included in the article. The accepted manuscripts will be made shared through Pubmed Central, as recommended by the NIH guidelines and policy on Sharing of Research Data.

*Supporting information*—This article contains supporting information (11–13, 39, 40).

*Acknowledgments*—We are thankful to Dr John Lloyd, NIDDK for Mass spec facility; Dr Michal Jarnik, NICHD for TEM; and Dr Diana Bianchi, NHGRI, NICHD for fluorescence plate reader.

*Author contributions*—T. M. writing–original draft; T. M., J. S., and A. B. methodology; T. M. investigation; T. M. formal analysis; T. M., J. S., and A. B. conceptualization; A. B. writing–review and editing; A. B. supervision; A. B. project administration; A. B. funding acquisition.

*Funding and additional information*—This research is supported by the Intramural Research Program of the Eunice Kennedy Shriver National Institute of Child Health and Human Development (NICHD), National Institutes of Health (A. B.). The content is solely the responsibility of the authors and does not necessarily represent the official views of the National Institutes of Health.

*Conflict of interest*—The authors declare that they have no conflicts of interest with the contents of this article.

*Abbreviations*—The abbreviations used are: AEBSF, 4-(2-aminoethyl)-benzenesulfonyl fluoride hydrochloride; DDM, n-dodecyl-β-D-maltopyranoside; DIPEA, N,N-Diisopropylethylamine; DMEM, Dulbecco's modified Eagle's medium; DMF, N,N-dimethylformamide; EGFR, epidermal growth factor receptor; $GABA_A$, γ-aminobutyric acid type A; PSD-95, postsynaptic density protein-95; SARS-CoV-2, severe acute respiratory syndrome coronavirus 2; SEC, size-exclusion chromatography; TCEP, tris(2- carboxyethyl) phosphine; βME, β-Mercaptoethanol.

## References


1. Jiang, H., Zhang, X., Chen, X., Aramsangtienchai, P., Tong, Z., and Lin, H. (2018) Protein lipidation: occurrence, mechanisms, biological functions, and enabling technologies. *Chem. Rev.* **118**, 919–988
2. Blanc, M., David, F. P. A., and van der Goot, F. G. (2019) SwissPalm 2: protein S-palmitoylation database. *Methods Mol. Biol.* **2009**, 203–214
3. Lobo, S., Greentree, W. K., Linder, M. E., and Deschenes, R. J. (2002) Identification of a ras palmitoyltransferase in Saccharomyces cerevisiae. *J. Biol. Chem.* **277**, 41268–41273
4. Roth, A. F., Feng, Y., Chen, L., and Davis, N. G. (2002) The yeast DHHC cysteine-rich domain protein Akr1p is a palmitoyl transferase. *J. Cell Biol.* **159**, 23–28
5. Malgapo, M. I. P., and Linder, M. E. (2021) Substrate recruitment by zDHHC protein acyltransferases. *Open Biol.* **11**, 210026
6. Mesquita, F. S., Abrami, L., Samurkas, A., and van der Goot, F. G. (2024) S-acylation: an orchestrator of the life cycle and function of membrane proteins. *FEBS J.* **291**, 45–56
7. Martin, B. R., Wang, C., Adibekian, A., Tully, S. E., and Cravatt, B. F. (2011) Global profiling of dynamic protein palmitoylation. *Nat. Methods* **9**, 84–89
8. Ko, P. J., and Dixon, S. J. (2018) Protein palmitoylation and cancer. *EMBO Rep.* **19**, e46666
9. Wlodarczyk, J., Bhattacharyya, R., Dore, K., Ho, G. P. H., Martin, D. D. O., Mejias, R., *et al.* (2024) Altered protein palmitoylation as disease mechanism in neurodegenerative disorders. *J. Neurosci.* **44**, e1225242024
10. Stix, R., Lee, C. J., Faraldo-Gomez, J. D., and Banerjee, A. (2020) Structure and mechanism of DHHC protein acyltransferases. *J. Mol. Biol.* **432**, 4983–4998
11. Swarthout, J. T., Lobo, S., Farh, L., Croke, M. R., Greentree, W. K., Deschenes, R. J., *et al.* (2005) DHHC9 and GCP16 constitute a human protein fatty acyltransferase with specificity for H- and N-Ras. *J. Biol. Chem.* **280**, 31141–31148
12. Rana, M. S., Kumar, P., Lee, C. J., Verardi, R., Rajashankar, K. R., and Banerjee, A. (2018) Fatty acyl recognition and transfer by an integral membrane S-acyltransferase. *Science* **359**, eaao6326
13. Mitchell, D. A., Mitchell, G., Ling, Y., Budde, C., and Deschenes, R. J. (2010) Mutational analysis of Saccharomyces cerevisiae Erf2 reveals a two-step reaction mechanism for protein palmitoylation by DHHC enzymes. *J. Biol. Chem.* **285**, 38104–38114
14. Gottlieb, C. D., Zhang, S., and Linder, M. E. (2015) The cysteine-rich domain of the DHHC3 palmitoyltransferase is palmitoylated and contains tightly bound zinc. *J. Biol. Chem.* **290**, 29259–29269
15. Jennings, B. C., and Linder, M. E. (2012) DHHC protein S-acyltransferases use similar ping-pong kinetic mechanisms but display different acyl-CoA specificities. *J. Biol. Chem.* **287**, 7236–7245
16. Rocks, O., Gerauer, M., Vartak, N., Koch, S., Huang, Z. P., Pechlivanis, M., *et al.* (2010) The palmitoylation machinery is a spatially organizing system for peripheral membrane proteins. *Cell* **141**, 458–471
17. Puthenveetil, R., Lun, C. M., Murphy, R. E., Healy, L. B., Vilmen, G., Christenson, E. T., *et al.* (2021) S-acylation of SARS-CoV-2 spike protein: mechanistic dissection, in vitro reconstitution and role in viral infectivity. *J. Biol. Chem.* **297**, 101112
18. Mesquita, F. S., Abrami, L., Sergeeva, O., Turelli, P., Qing, E., Kunz, B., *et al.* (2021) S-acylation controls SARS-CoV-2 membrane lipid organization and enhances infectivity. *Dev. Cell* **56**, 2790–2807.e2798
19. Lin, Y. H., Doms, A. G., Cheng, E., Kim, B., Evans, T. R., and Machner, M. P. (2015) Host cell-catalyzed S-palmitoylation mediates golgi targeting of the Legionella ubiquitin ligase GobX. *J. Biol. Chem.* **290**, 25766–25781
20. Runkle, K. B., Kharbanda, A., Stypulkowski, E., Cao, X. J., Wang, W., Garcia, B. A., *et al.* (2016) Inhibition of DHHC20-mediated EGFR palmitoylation creates a dependence on EGFR signaling. *Mol. Cell* **62**, 385–396
21. Yang, Y., Hsu, J. M., Sun, L., Chan, L. C., Li, C. W., Hsu, J. L., *et al.* (2019) Palmitoylation stabilizes PD-L1 to promote breast tumor growth. *Cell Res* **29**, 83–86
22. Yao, H., Lan, J., Li, C., Shi, H., Brosseau, J. P., Wang, H., *et al.* (2019) Inhibiting PD-L1 palmitoylation enhances T-cell immune responses against tumours. *Nat. Biomed. Eng.* **3**, 306–317
23. Rathenberg, J., Kittler, J. T., and Moss, S. J. (2004) Palmitoylation regulates the clustering and cell surface stability of GABAA receptors. *Mol. Cell Neurosci* **26**, 251–257
24. Keller, C. A., Yuan, X., Panzanelli, P., Martin, M. L., Alldred, M., Sassoe-Pognetto, M., *et al.* (2004) The gamma2 subunit of GABA(A) receptors is a substrate for palmitoylation by GODZ. *J. Neurosci.* **24**, 5881–5891
25. Linder, M. E., Middleton, P., Hepler, J. R., Taussig, R., Gilman, A. G., and Mumby, S. M. (1993) Lipid modifications of G proteins: alpha subunits are palmitoylated. *Proc. Natl. Acad. Sci. U S A.* **90**, 3675–3679
26. Tsutsumi, R., Fukata, Y., Noritake, J., Iwanaga, T., Perez, F., and Fukata, M. (2009) Identification of G protein alpha subunit-palmitoylating enzyme. *Mol. Cell. Biol.* **29**, 435–447
27. Fukata, M., Fukata, Y., Adesnik, H., Nicoll, R. A., and Bredt, D. S. (2004) Identification of PSD-95 palmitoylating enzymes. *Neuron* **44**, 987–996
28. Lemonidis, K., Gorleku, O. A., Sanchez-Perez, M. C., Grefen, C., and Chamberlain, L. H. (2014) The Golgi S-acylation machinery comprises zDHHC enzymes with major differences in substrate affinity and S-acylation activity. *Mol. Biol. Cell.* **25**, 3870–3883
29. Denisov, I. G., and Sligar, S. G. (2016) Nanodiscs for structural and functional studies of membrane proteins. *Nat. Struct. Mol. Biol.* **23**, 481–486
30. Stix, R., Song, J., Banerjee, A., and Faraldo-Gomez, J. D. (2020) DHHC20 palmitoyl-transferase reshapes the membrane to foster catalysis. *Biophys. J.* **118**, 980–988
31. Lemonidis, K., Sanchez-Perez, M. C., and Chamberlain, L. H. (2015) Identification of a novel sequence motif recognized by the ankyrin repeat domain of zDHHC17/13 S-acyltransferases. *J. Biol. Chem.* **290**, 21939–21950
32. Puthenveetil, R., Gomez-Navarro, N., and Banerjee, A. (2022) Access and utilization of long-chain fatty acyl-coA by zDHHC protein acyltransferases. *Curr. Opin. Str. Biol.* **77**, 102463
33. Rana, M. S., Wang, X., and Banerjee, A. (2018) An improved strategy for fluorescent tagging of membrane proteins for overexpression and purification in mammalian cells. *Biochemistry* **57**, 6741–6751

34. Coin, I., Beyermann, M., and Bienert, M. (2007) Solid-phase peptide synthesis: from standard procedures to the synthesis of difficult sequences. *Nat. Protoc.* **2**, 3247–3256
35. Mondal, T., and Mandal, B. (2019) Engineered peptidic constructs metabolize amyloid beta by self-assembly-driven reactions. *Chem. Commun. (Camb)* **55**, 4933–4936
36. Long, S. B., Tao, X., Campbell, E. B., and MacKinnon, R. (2007) Atomic structure of a voltage-dependent K+ channel in a lipid membrane-like environment. *Nature* **450**, 376–382
37. Stanley, C. J., and Perham, R. N. (1980) Purification of 2-oxo acid dehydrogenase multienzyme complexes from ox heart by a new method. *Biochem. J.* **191**, 147–154
38. Ritchie, T. K., Grinkova, Y. V., Bayburt, T. H., Denisov, I. G., Zolnerciks, J. K., Atkins, W. M., *et al.* (2009) Chapter 11 - reconstitution of membrane proteins in phospholipid bilayer nanodiscs. *Methods Enzymol.* **464**, 211–231
39. Mitchell, D. A., Pendleton, L. C., and Deschenes, R. J. (2019) In vitro assays to monitor the enzymatic activities of zDHHC protein acyltransferases. *Methods Mol Biol* **2009**, 169–177
40. Lanyon-Hogg, T., Ritzefeld, M., Sefer, L., Bickel, J. K., Rudolf, A. F., Panyain, N., *et al.* (2019) Acylation-coupled lipophilic induction of polarisation (Acyl-cLIP): a universal assay for lipid transferase and hydrolase enzymes. *Chem. Sci.* **10**, 8995–9000